2023-05-15

Ocean acidification stunts molluscan growth at CO2 seeps

Zhao, L

http://hdl.handle.net/10026.1/20492

10.1016/j.scitotenv.2023.162293
Science of The Total Environment
Elsevier BV

Ocean acidification stunts molluscan growth at CO_2 seeps

Liqiang Zhao [a, b, *], Ben P. Harvey [c, *], Tomihiko Higuchi [b], Sylvain Agostini [c], Kentaro Tanaka [b], Naoko Murakami-Sugihara [b], Holly Morgan [d], Phoebe Baker [d], Jason M. Hall-Spencer [c, d], Kotaro Shirai [b]

[a] *College of Fisheries, Guangdong Ocean University, Zhanjiang 524088, China*

[b] *Atmosphere and Ocean Research Institute, The University of Tokyo, Chiba 277-8564, Japan*

[c] *Shimoda Marine Research Center, University of Tsukuba, Shimoda 415-0025, Japan*

[d] *School of Biological and Marine Sciences, University of Plymouth, Plymouth PL4 8AA, UK*

***** *Co-corresponding authors*:

lzhao@gdou.edu.cn (L.Z.); ben.harvey@shimoda.tsukuba.ac.jp (B.P.H.)

Abstract

Ocean acidification can severely affect bivalve molluscs, especially their shell calcification. Assessing the fate of this vulnerable group in a rapidly acidifying ocean is therefore a pressing challenge. Volcanic CO_2 seeps are natural analogues of future ocean conditions that offer unique insights into the scope of marine bivalves to cope with acidification. Here, we used a 2-month reciprocal transplantation of the coastal mussel *Septifer bilocularis* collected from reference and elevated pCO_2 habitats to explore how they calcify and grow at CO_2 seeps on the Pacific coast of Japan. We found significant decreases in condition index (an indication of tissue energy reserves) and shell growth of mussels living under elevated pCO_2 conditions. These negative responses in their physiological performance under acidified conditions were closely associated with changes in their food sources (shown by changes to the soft tissue $\delta^{13}C$ and $\delta^{15}N$ ratios) and changes in their calcifying fluid carbonate chemistry (based on shell carbonate isotopic and elemental signatures). The reduced shell growth rate during the transplantation experiment was further supported by shell $\delta^{13}C$ records along their incremental growth layers, as well as their smaller shell size despite being of comparable ontogenetic ages (5-7 years old, based on shell $\delta^{18}O$ records). Taken together, these findings demonstrate how ocean acidification at CO_2 seeps affects mussel growth and reveal that lowered shell growth helps them survive stressful conditions.

Keywords: Climate change; Bivalves; Calcification; Acclimation; Sclerochronology

1. Introduction

Since the Industrial Revolution, the atmospheric concentration of carbon dioxide (CO_2) has increased at an unprecedented rate from about 280 ppm in 1750 to 410 ppm in 2018, due mainly to human activities such as burning fossil fuels (Blunden et al., 2018). About one-third of all anthropogenic CO_2 has entered the ocean, causing decreases in seawater pH, carbonate ion (CO_3^{2-}) concentration, and saturation state of calcium carbonate ($CaCO_3$), and increases in the partial pressure of CO_2 (pCO_2) and bicarbonate ion (HCO_3^-) concentration (Caldeira and Wickett, 2003). These fundamental changes in seawater chemistry, known as ocean acidification (OA), can severely affect most marine bivalves, one of the most ecologically and economically important taxonomic groups in global marine ecosystems (e.g., Ekstrom et al., 2015; Leung et al., 2020a; Melzner et al., 2020; Martins et al. 2021; Leung et al., 2022). In particular, the ability of marine bivalves to calcify, which in turn controls individual growth, development, defense and survival, is highly sensitive to CO_2-driven changes in seawater carbonate system (e.g., Waldbusser et al., 2014; Thomsen et al., 2017; Zhao et al., 2017a; Rajan et al., 2021). Hence, obtaining an integrated understanding of how OA affects the calcification physiology can represent an important step forward in assessing the fate of marine bivalves in a rapidly acidifying ocean.

The calcification of marine bivalves can be thought of as a step-by-step process, and OA can likely affect each of these separate steps. This includes OA substantially affecting the source and pathway of calcifying substrates such as Ca^{2+} and HCO_3^- ions

transported from ambient seawater to the calcifying front (Lu et al., 2018; Sillanpää et al., 2018; Zhao et al., 2018a), and the removal of protons generated during the $CaCO_3$ precipitation (Zhao et al., 2017b; Liu et al., 2020). Likewise, the synthesis of organic matrix for the $CaCO_3$ crystallization and periostracum formation can succumb under acidified conditions (Hüning et al., 2013; Ramajo et al., 2016). Nevertheless, continuous *in situ* monitoring of changes at the calcifying front remains an extremely challenging task, due to the thin extrapallial space located between the inner shell layer and mantle tissue (Marin et al., 2012; He et al., 2023). Alternatively, a suite of geochemical proxies archived in shell carbonates hold great potential for estimating responses to ocean acidification (Levin et al., 2015). When exposed to elevated pCO_2, for example, the relative contribution of seawater carbon and metabolic carbon to the calcifying pool can be examined by shell carbon isotopes (Lu et al., 2018; Zhao et al., 2018a). The amount of boron and uranium incorporated into shells are inversely related to the pH in the calcifying fluid (Frieder et al., 2014; Zhao et al., 2018b), and incorporation of sodium into shells can be closely related to activities of ionic exchangers by which marine bivalves regulate the acid-base status at the site of calcification (Zhao et al., 2017a, 2017b). While these significant advances have been made in disentangling processes constraining the calcification sensitivity to OA, as demonstrated above, little effort has been devoted to integrating how long-term OA will affect calcification processes when considered together, thus constraining our ability to assess the extent of the calcification plasticity in response to OA.

Experiments performed across multiple generations can likely provide a means to understand the acclimation potential and mechanistic basis of marine bivalves in a rapidly acidifying ocean. A growing body of transgenerational studies, for example, demonstrates that marine bivalves (at least species hitherto studied) may have the ability to respond plastically and acclimate rapidly to OA scenarios projected by the end of this century (e.g., Ross et al., 2016; Thomsen et al., 2017; Byrne et al., 2020; Zhao et al., 2020a). However, despite the great potential of transgenerational experiments in examining whether bivalves can keep up with the pace of OA, their relatively long generation times (from months to years) and complex life cycles complicate multigenerational experiments. In addition, almost all transgenerational experiments have been carried out under simulated conditions. In the face of multiple stressors and complexities of the nature, whether rapid transgenerational acclimation can be still maintained remains unknown. Hence, approaches which can document the acclimation plasticity under environmentally realistic scenarios are in high demand.

A space-for-time approach opens a promising avenue in examining the extent to which marine bivalves have the capacity to acclimate to OA. Synchronic comparisons of individuals naturally growing along large gradients of pCO_2 and pH to substitute space for time, so-called the space-for-time substitution (Reusch, 2014), can likely capture long-term ecological relevance and more accurately assess the fate of key species, populations, and ecosystems under projected OA scenarios. Naturally CO_2-

enriched habitats, especially volcanic CO_2 seeps that can generate consistently acidic conditions throughout the year, are increasingly used as natural analogues of future ocean acidification conditions (Feely et al., 2008; Hall-Spencer et al., 2008; Rastrick et al., 2018). Within the framework of space-for-time substitution, the large predatory gastropod *Charonia lampas* living in CO_2 seeps off Shikine Island (Japan) and the widespread Mediterranean mollusc *Hexaplex trunculus* in Vulcano Island CO_2 seeps (Italy) show little ability to compensate for corrosive effects of seawater acidification on shell mineralization (Harvey et al., 2016, 2018). Nevertheless, contrasting findings have recently been observed in molluscs inhabiting CO_2 seeps in the south-western Pacific, where the herbivorous gastropod *Eatoniella mortoni* produces thicker, more crystalline, and mechanically resilient shells for compensatory growth (Leung et al., 2019). These discrepancies among CO_2 seep habitats can most likely be attributed to differences in duration, frequency, and intensity of acidification (Aiuppa et al., 2021). To the best of our knowledge, nevertheless, only a few studies have used natural CO_2 seeps to advance our knowledge of the acclimation of marine bivalves to projected OA scenarios (e.g., Hahn et al. 2012; Agostini et al. 2018; Martins et al. 2021).

Japanese volcanic CO_2 seeps, especially those off Shikine Island, have recently been developed as natural analogues of future oceanic conditions to show how marine organisms and ecosystems respond and acclimate to OA (e.g., Inoue et al., 2013; Agostini et al., 2018, 2021; Cattano et al., 2020; Harvey et al., 2018, 2020, 2021a, 2021b). The intertidal rocky shore communities along the coast of Shikine

130 Island are composed predominantly of calcifying species (mussels, oysters, barnacles,
131 coralline algae, etc.), whose abundance and distribution vary in both space and time.
132 Surveys using quadrats (25 × 25 cm) showed that the population density of intertidal
133 mussels near the CO_2 seeps was reduced compared to outside the seeps (from 7 ± 13
134 individuals to 2 ± 3 individuals; Agostini et al., 2018), indicating that they may be
135 negatively impacted by elevated pCO_2 conditions and hence sparking our interest in
136 testing whether, and to what extent, bivalves living near Shikine Island CO_2 seeps
137 have the ability to acclimate under these naturally acidified conditions.
138
139 Here, we aimed at gaining a better understanding of the acclimation potential of
140 the widely distributed mussel *Septifer bilocularis* along the coast of Shikine Island to
141 ocean acidification. Firstly, we performed a 2-month reciprocal transplant of mussels
142 between an elevated pCO_2 area and an adjacent reference pCO_2 area to assess their
143 physiological performance. Secondly, we performed ultra-high-resolution temporal
144 analysis (on a subset of individuals) of shell geochemistry along growth layers to gain
145 temporal information for their lifespan. Geochemical approaches, such as stable
146 carbon and nitrogen isotopic and trace elemental analyses which hold great promise
147 to disentangle calcification responses of marine bivalves to ocean acidification in
148 temporal context (as reviewed by Zhao et al., 2020a), were employed to obtain an
149 integrated insights into mechanisms behind mussel calcification and associated
150 physiological processes. Our findings provide a more comprehensive understanding
151 about how mussels respond and likely acclimate in a rapidly acidifying ocean.

2. Materials and methods

2.1. Study area

Shikine Island (34°19'9" N, 139°12'18" E) is a volcanic island located off the Izu peninsula in Japan. The shore of the island is composed of crustal rocks varying in size with the tidal range less than 2 m, and near CO_2 seeps the water depth is approximate 4 m during high tides. As schematically illustrated in Fig. 1, our two low intertidal sites, elevated pCO_2 area and reference pCO_2 area, have well characterized carbonate chemistry (e.g., Agostini et al., 2015, 2018; Cattano et al., 2020; Harvey et al., 2018, 2020, 2021a, 2021b; Witkowski et al., 2019). The carbonate chemistry of the two sites at the time of the current study are published in Harvey et al. (2020). Briefly, seawater pH_T, temperature and salinity of the two sites were recorded through *in situ* measurements of the subtidal environment using a multisensor (WQC-24, TOA-DKK, Japan). Total alkalinity samples were collected as discrete samples and measured by titration (916 Ti-Touch, Metrohm) with 0.1 mol l^{-1} HCl. Seawater carbonate system parameters were calculated from temperature, salinity, pH_T and total alkalinity using the software CO2SYS (Pierrot et al., 2006). The reference pCO_2 area had a mean pH_T of 8.041 ± 0.067 (SD) and the elevated pCO_2 area had a mean pH_T of 7.719 ± 0.095 (SD). The elevated pCO_2 area represents an end of the present century projection for reductions in pH under the Representative Concentration Pathway 8.5 scenario (IPCC, 2013), and had the same temperature, salinity, dissolved oxygen, total alkalinity, nutrients and depth as the reference site

174 (Agostini et al., 2015, 2018; Harvey et al., 2019, 2021a), as well as the same carbon
175 isotopic ratio of dissolved inorganic carbon (Fig. 1) relative to the reference pCO_2
176 area used for comparison. The gas emitted from the seeps is 98% CO_2 (Agostini et al.,
177 2015). The annual range of sea surface temperature varies from 14 to 28 °C and
178 salinity remains constant at ca. 34 over time (Agostini et al., 2018; Harvey et al.
179 2021a).
180
181 ***2.2. Study organism***
182 Mytilidae represent some of the most conspicuous marine bivalves within the
183 intertidal and shallow subtidal zones (Morton, 2019). Species of *Septifer* (Récluz,
184 1848), along with many warm-water Mytilidae, are far less well studied when
185 compared to genera such as *Mytilus* and *Perna* (Morton et al. 2020). *Septifer*
186 *bilocularis* (Linnaeus, 1758), our study organism, is located along the coasts of
187 mainland Japan, as well as in the Indo-West-Pacific (Higo et al. 1999). Individuals of *S.*
188 *bilocularis* have a thick, ovally elongate shell that is ventrally concave, dorsally
189 peaked with a rounded posterior margin with terminal beaks (Morton et al. 2020).
190 The shell valves are covered by a thick periostracum over fine radially divaricating
191 lirae (Morton et al. 2020). This species was the dominant mussel within our study
192 site, and yet little else about its ecology has previously been described. Individuals of
193 *S. bilocularis* in Hong Kong are subtidal and associated with coral heads (Dudgeon
194 and Morton, 1982), whereas individuals (shell length of 23–28 mm and body weight
195 of 2.3–2.5 g) in our study site are found attached by byssal threads to the rocky

substratum in the low intertidal zone.

2.3. Experimental setup

Adults of *S. bilocularis* inhabiting the low intertidal zone in the elevated pCO_2 and reference pCO_2 areas were randomly collected, individually labelled with a reference number using queen bee marking tags (E.H. Thorne Ltd., UK), and reciprocally transplanted for two months (mid-April to mid-June 2019) using a two-way orthogonal experimental design (as schematically illustrated in Fig. 1). This design therefore includes procedural controls where some individuals were transplanted back into the same site they were collected from. Redeployment of individuals for the two-month reciprocal transplantation was achieved by placing them inside cages (green mesh, 20 × 10 × 4 cm, 1 cm mesh size) which were attached to the substratum with anchor bolts in locations next to where the mussel individuals were originally collected in the low intertidal zone (two cages per site) at the same tidal height (with a maximum tidal depth of around 2.0 m during spring tides). Each cage contained five individuals collected from reference pCO_2 conditions and five individuals collected from elevated pCO_2 conditions (individuals were randomly assigned to the four cages). Seawater samples for the stable carbon isotope ratio ($\delta^{13}C$) analysis were collected using 20-ml glass vials and poisoned with two drops of the supersaturated mercury chloride solution to prevent any biological interference.

Following the *in situ* transplant experiment, two individuals from each site

218 (elevated pCO_2 and reference pCO_2) were used for high-resolution analysis over their
219 lifespan to identify ontogenetic age, annual growth rate, and geochemical properties
220 via stable isotopic analysis (described in greater detail below). These individuals were
221 selected from the reciprocal transplant experiment, at random (one from each cage),
222 using only those procedural control individuals that had been collected from, and
223 transplanted back into the same site.
224
225 ***2.4. Sample collection and individual analysis***
226 Following our *in situ* transplant experiment, all specimens were carefully cleaned and
227 then frozen at –20 °C. Four or five individuals from each of the four treatments of the
228 reciprocal transplant were randomly sampled and dissected using a scalpel for
229 analysis. The whole soft tissue of each mussel was washed with Milli-Q water (18.2
230 mΩ), freeze-dried for 48 h and then weighed, and the shell air-dried and weighed.
231 The condition index (CI) of each sample was calculated using the equation (1) (Lucas
232 and Beninger, 1985).
233
234 $CI = dtw/dsw \times 100$ .....(1)
235
236 where CI is the condition index, and dtw and dsw represent the dry soft tissue
237 weight (g) and dry shell weight (g), respectively.
238
239 The newly formed shell portion of each mussel was analyzed to examine its daily

growth rate. Specifically, mussel shells were sectioned to accurately analyze the rate of shell growth and thickness of periostracum formation during the experiment. The right valve of each shell was embedded in epoxy resin and along the axis of maximum growth two three-millimeter-thick sections were cut using a low-speed diamond saw (Isomet 1000, Buehler, Lake Bluff, IL, United States). Afterward, both sections were mounted on glass slides, ground with 70 and 13 µm diamond cup whetstones, respectively, polished with 0.3 µm alumina powder, and then ultrasonically washed with Milli-Q water (18.2 mΩ) to remove any adhering particles. Photographs of polished shell sections were taken using a digital microscope (KEYENCE VHX-2000) and the amount of newly formed shell portions (as determined by internal growth bands; Zhao et al., 2019a) and also thickness of corresponding periostracum were analyzed using an image processing software ImageJ. The average daily rate of mussel shell growth during the experiment was subsequently computed.

To perform high-resolution analysis across the lifespan of the mussel, the mussels subsampled from the reciprocal transplant experiment were used (one mussel from each cage in the elevated pCO_2 area, and one mussel from each cage in the reference pCO_2 area). We only used individuals collected from and transplanted back into the same site. These mussels were soaked in 0.5 wt% HCl overnight at room temperature to prevent shell surface contamination (Zhao et al., 2019b). Carbonate samples from the left valve of each mussel were then milled along the axis of maximum shell growth at approximately 0.1-0.3 mm resolution for subsequent

geochemical analysis.

2.5. Isotopic analysis via EA-IRMS and CF-IRMS

Approximately 2 mg of soft tissue from each mussel was homogenized and weighed into a tin capsule, tightly folded, and then analyzed using an elemental analyzer (EA; vario MICRO cube, Elementar, Germany) interfaced to an isotope ratio mass spectrometer (IRMS; IsoPrime100, IsoPrime, UK) at the Atmosphere and Ocean Research Institute (AORI), University of Tokyo. Stable carbon and nitrogen isotope ratios ($\delta^{13}C$ and $\delta^{15}N$) were reported related to the standards (Vienna Pee Dee Belemnite (VPDB) and the atmospheric nitrogen, respectively), and expressed in the conventional delta (δ) notation in per mil (‰). Measured $\delta^{13}C$, $\delta^{15}N$ and C/N ratio were calibrated respectively against standards (L-alanine (AZ101SS13), Shoko Scientific; $\delta^{13}C$ = –19.6 ‰, $\delta^{15}N$ = 13.7, and C/N = 3.0). Throughout the analysis, the NIST SRM 2976 (National Institute of Standards and Technology, United States) was used to monitor instrumental conditions. The reproducibility was better than 0.28 ‰ for $\delta^{13}C$ (1 δ) and 0.10 ‰ for $\delta^{15}N$ (1 δ).

To measure stable carbon and oxygen isotope ratios ($\delta^{13}C$ and $\delta^{18}O$) of the shell, approximately 100 µg of carbonate powder milled from the newly formed shell portion was weighed into a glass vial and then reacted with 100 % phosphoric acid at 72 °C in a helium-flushed borosilicate exetainer for one hour. Liberated CO_2 gas was analyzed using a Thermo Finnigan Delta V Plus continuous flow-isotope ratio mass

spectrometer (CF-IRMS) coupled to a Thermo Finnigan GasBench II at AORI. Measured $\delta^{13}C$ and $\delta^{18}O$ data were calibrated against NBS-19 ($\delta^{13}C$ = +1.95 ‰; $\delta^{18}O$ = –2.20 ‰). Shell $\delta^{13}C$ and $\delta^{18}O$ values were calculated against VPDB, reported in δ-notation and then given as ‰. Profiles of $\delta^{18}O_{shell}$ provide a chronological framework, with each shell portion placed into a temporal context allowing the ontogenetic age of each specimen to be determined. By doing so, the implications of ontogeny in the interpretation of results from reciprocal transplantation can be substantially eliminated. The reproducibility was better than 0.05 ‰ for $\delta^{13}C$ (1 δ) and 0.23 ‰ for $\delta^{18}O$ (1 δ). Seawater $\delta^{13}C$ analysis was performed using CF-IRMS, calibrated and calculated in the same manner as shell $\delta^{13}C$ values.

2.6. Elemental analysis via LA-ICP-MS

Concentrations of boron (B), Sodium (Na), Magnesium (Mg), Phosphorus (P), Potassium (K), Strontium (Sr), Barium (Ba), and Uranium (U) in polished shell sections were analyzed by laser ablation inductively coupled plasma mass spectrometry (LA-ICP-MS) in 'spot' mode at AORI. Three to six discrete spots based on the incremental length in the newly formed shell portion during the experiment were set in each shell. Analyses were performed with an excimer-based laser ablation system (NWR-193, New Wave Research, Fremont, CA, United States) connected to ICP-MS (7700 CS, Agilent, Tokyo, Japan). The laser was operated at a pulse rate of 10 Hz, pulse energy of 1.8 mJ, and beam diameter of 100 µm. Helium was used as the carrier gas. Prior to each ablation backgrounds were analyzed for 7 s, and subsequent ablation time was

306 15 s followed by 25 s wash out. The signal intensity of ions (^{10}B, ^{23}Na, ^{24}Mg, ^{31}P, ^{39}K,
307 ^{43}Ca, ^{88}Sr, ^{138}Ba, ^{238}U) was calculated by subtracting the background level of trace
308 elements empirically obtained with the 0 % laser output set. ^{43}Ca was used as
309 internal standard and the element-to-^{43}Ca ratio was computed and compared to the
310 standard reference material signal intensity. NIST SRM 612 (synthetic glass) was used
311 as an external standard, and giant clam powder JCt-1 and coral powder JCp-1
312 (National Institute of Advanced Industrial Science and Technology, Tsukuba, Japan)
313 were measured as quality control materials to confirm accuracy. Calculations on trace
314 element-to-calcium ratio were based on analyses of NIST SRM 612. To monitor the
315 instrumental drift, all reference materials were analyzed after every 10-20 samples.
316

317 ***2.7. Statistical analysis***

318 The $\delta^{13}C$ composition of bivalve shells is controlled by seawater $\delta^{13}C_{DIC}$, the $\delta^{13}C$ of
319 metabolically generated CO_2, as well as the proportion of metabolic CO_2
320 incorporated into shell carbonate (McConnaughey and Gillikin, 2008). Hence,
321 determination of the relative contribution of metabolic carbon can be achieved
322 according to the following equation (2) described by McConnaughey et al. (1997).
323

324 $$\%C_M = (\delta^{13}C_{shell} - \varepsilon_{cal\text{-}b} - \delta^{13}C_{DIC})/(\delta^{13}C_M - \delta^{13}C_{DIC}) \times 100 \quad (2)$$

325

326 where $\%C_M$ is the percentage of metabolic carbon incorporated into shell carbonate.
327 $\delta^{13}C_{shell}$, $\delta^{13}C_{DIC}$ and $\delta^{13}C_M$ represent the $\delta^{13}C$ of shell carbonate, seawater dissolved

328 inorganic carbon (DIC) and metabolic carbon, respectively, and $\varepsilon_{cal\text{-}b}$ represents the
329 enrichment factor between calcite and bicarbonate (1 ‰ calculated by Romanek et
330 al., 1992). In the present study, the $\delta^{13}C$ ratios of mussel soft tissues were employed
331 to approximate $\delta^{13}C_M$ according to McConnaughey et al. (1997).
332
333 All data generated following reciprocal transplantation were analyzed using the
334 IBM SPSS Statistics version 19.0 (SPSS Inc., Chicago, IL, USA). Shapiro-Wilk's test and
335 Levene's F-test were performed to examine the normal distribution (normality) and
336 equal variance among groups (homoscedasticity) of experimental data. A fixed-
337 effects analysis of variance (ANOVA) model of pCO_2 (2 levels, reference pCO_2 and
338 elevated pCO_2) and origin (2 levels, reference pCO_2 and elevated pCO_2) was used for
339 the analysis. Following the two-way ANOVA, a Fisher's Least Significant Difference
340 (LSD) post-hoc test was performed to test the significance of experimental data
341 among groups designated according to the two-way orthogonal experimental design.
342 Statistical significance was set at $p < 0.05$. The fixed-effects model was initially
343 compared to a mixed-effects model using the 'transplant cage' as a random-effect for
344 each endpoint measurement. In all cases, the fixed effects model did not significantly
345 differ from the mixed effects model and demonstrated lower AIC scores. As such, the
346 more parsimonious fixed-effects model was employed.
347

348 ## 3. Results

349 ### 3.1. Growth performance following transplantation

350 No mortality was recorded over the course of the transplant experiment. No
351 statistically significant differences in physiological traits were observed for mussels
352 transplanted within the same areas (i.e., elevated pCO_2 or reference pCO_2
353 conditions), irrespective of their origin under elevated or reference pCO_2 conditions
354 ($p > 0.05$; Figs. 2a and 2b). Residing in elevated pCO_2 conditions significantly affected
355 the physiological performance of the mussels, as best exemplified by significant
356 decreases in their condition index ($p < 0.05$; Fig. 2a) and shell growth ($p < 0.05$; Fig.
357 2b). Nevertheless, neither pCO_2 conditions nor the reciprocal transplantation, and
358 their interaction, significantly affected the thickness of mussel shell periostracum
359 ($p > 0.05$; Fig. 2c).
360

361 **3.2. Somatic stable isotopic signatures following transplantation**

362 Mussels collected under reference pCO_2 conditions showed significantly higher
363 $\delta^{13}C_{soft\ tissue}$ values than those inhabiting elevated pCO_2 conditions ($p < 0.05$; Fig. 3a).
364 Mussel $\delta^{15}N_{soft\ tissue}$ signatures were only significantly affected by reciprocal
365 transplantation, with values significantly higher in mussels collected from reference
366 pCO_2 areas than those typically residing in elevated pCO_2 areas when experimentally
367 exposed to elevated pCO_2 ($p < 0.05$; Fig. 3b). Mussel C/N ratios were not significantly
368 affected by either pCO_2 conditions or reciprocal transplantation ($p > 0.05$; Fig. 3c).
369

370 **3.3. Shell geochemical properties following transplantation**

371 While the shells of mussels collected from reference pCO_2 areas had consistently

372 lower $\delta^{13}C_{shell}$ values in comparison with those in elevated pCO_2 areas (Fig. 4a), no
373 significant effect of reciprocal transplantation was found ($p > 0.05$). $\delta^{13}C_{shell}$ ratios
374 were also not significantly affected by pCO_2 conditions ($p > 0.05$). Interaction
375 between these two factors exhibited significant effects on $\delta^{18}O_{shell}$ ratios ($p < 0.05$;
376 Fig. 4b). Under acidified conditions, mussels collected from reference pCO_2 areas
377 showed significantly lower $\delta^{18}O_{shell}$ values than those previously inhabiting elevated
378 pCO_2 areas ($p < 0.05$). Furthermore, as shown in Fig. 4c, seawater DIC was
379 determined as the predominant source of shell carbonate, and its contribution to the
380 DIC pool at the site of calcification increased with increasing pCO_2 concentration.
381
382 Element-to-calcium ratios of mussel shells following transplantation are shown
383 in Fig. 5. With increasing pCO_2 concentration, the amount of B (Fig. 5a) and U (Fig. 5h)
384 incorporated into shell carbonate decreased significantly ($p < 0.05$). Nevertheless,
385 the incorporations of Na (Fig. 5b), Mg (Fig. 5c), P (Fig. 5d), K (Fig. 5e), Sr (Fig. 5f), and
386 Ba (Fig. 5g) were not significantly affected by either pCO_2 conditions or the reciprocal
387 transplantation ($p < 0.05$).
388
389 **3.4. Analysis of shell geochemical properties over the lifespan**
390 As illustrated in Fig. 6a, high-resolution $\delta^{18}O_{shell}$ profiles of mussels originally living
391 under reference pCO_2 conditions and under elevated pCO_2 conditions were extracted
392 to constrain the ontogenetic age and rates of annual shell growth. Two mussels
393 randomly selected from the reference pCO_2 areas were 7-years-old and 5-years-old,

and those living in the elevated pCO_2 areas were 7-years-old and 6-years-old, respectively. Following placing each shell portion into a precise context, it is evident that across their entire lifespan mussels inhabiting elevated pCO_2 conditions grew at slower rates in comparison with those living under reference pCO_2 conditions (Fig. 6b). $\delta^{13}C_{shell}$ profiles provide consistent evidence of lower $\delta^{13}C_{shell}$ values in mussels living under reference pCO_2 conditions than those under elevated pCO_2 conditions (Fig. 6c).

4. Discussion

This is the first investigation of calcification responses of marine bivalves living around Japanese volcanic CO_2 seeps. Our observations of significantly lowered shell growth with increasing elevated pCO_2 indicate that mussels inhabiting elevated pCO_2 conditions have their shell formation negatively impacted and do not appear to be capable of rapidly acclimating to ocean acidification scenarios projected by the end of this century. These observations are in line with findings of drastically decreased abundance of bivalves with increasing levels of pCO_2 along the shore of Shikine Island (Agostini et al., 2018; Hall-Spencer et al., 2022). Similar observations have also been made at CO_2 seeps off islands of São Miguel and Faial in the North Atlantic Ocean, where the abundance, size and net-calcification of the bivalve (*Ervilia castanea*) were inversely related to pCO_2 levels (Martins et al., 2021). Yet, it is worth noting here that the declines in shell formation under elevated pCO_2 conditions at CO_2 seeps are at odds with previous conclusions that demonstrated marine bivalves inhabiting

416 naturally CO_2-enriched habitats, such as upwelling areas, can maintain the ability to
417 calcify by implementing compensatory mechanisms to mitigate effects of elevated
418 pCO_2 on shell calcification (e.g., Thomsen et al., 2017; Zhao et al., 2018b). In addition,
419 a growing body of transgenerational experiments has shown that a suite of
420 physiological processes underpinning the shell calcification can respond plastically
421 and acclimate rapidly to near-future OA scenarios (e.g., Fitzer et al., 2014; Parker et
422 al., 2015; Zhao et al., 2017b, 2018a). Given that volcanic CO_2 seeps can be more
423 reliably used as natural analogues of future oceanic conditions than many other
424 naturally CO_2-enriched systems (Rastrick et al., 2018), discrepancies among studies
425 deserve further attention. Hence, the elucidation of the underlying mechanisms
426 would represent a key leap forward in our understanding of how bivalves will
427 respond and acclimate in a rapidly acidifying ocean.
428

429 **4.1. Changes in dietary regimes of mussels under elevated pCO_2 conditions**

430 Following reciprocal transplantation, the condition index of the mussels, which is
431 widely used as an indication of the energy budget of bivalves (Lucas and Beninger,
432 1985), significantly decreased for those individuals held under the elevated pCO_2
433 conditions, indicating decreases in their energy reserves. Reduced energy reserves in
434 mussels under acidified conditions can partly be explained by changes in their dietary
435 regimes. For the first time, the present study utilized $\delta^{13}C$ and $\delta^{15}N$ ratios of mussel
436 soft tissues as dietary tracers and revealed marked shifts in food sources of mussels
437 living in reference and elevated pCO_2 areas. Significant changes in mussel $\delta^{13}C_{soft\ tissue}$

438 and $\delta^{15}N_{soft\ tissue}$ demonstrate changes in their principal food sources, which largely
439 stem from algal detritus (Zhao et al., 2013). Evidence in support of this interpretation
440 further comes from recent surveys around the same set of CO_2 seeps off Shikine
441 Island by Harvey et al. (2021a), according to which diatom algal turfs (*Biddulphia*
442 *biddulphiana*) largely replaced seaweeds and became the dominant habitat-forming
443 species around the CO_2 seeps, thereby potentially affecting components of organic
444 detritus. Given significant decreases in condition index and thereby energy reserves,
445 these shifts in food sources are likely much less beneficial for mussel calcification in
446 response to long-term elevated pCO_2 stress.
447
448 Nevertheless, it is worth noting here that only the combination of both quality
449 and quantity of food could reliably dictate dietary regimes of mussels at CO_2 seeps.
450 Without doubt, in the present study food sources of mussels varied as pCO_2 levels
451 rose, but it remains largely unknown how the nutritional quality of food (which can
452 be expressed in terms of C:N ratios) responded. At a CO_2 shallow vent system off
453 Ischia in the Mediterranean Sea, lowered C:N ratios of organic matter sources with
454 increasing pCO_2 levels can likely indicate higher nutritional quality of food produced
455 by primary producers (Ricevuto et al., 2015). Also, the dominant calorie-enriched turf
456 algae near CO_2 seeps in New Zealand had lower C:N ratio (and thus higher nutritional
457 quality) than that of seaweeds outside seeps (Leung et al., 2018, 2020). Presumably,
458 in the present study mussels might even consume higher nutritional quality of food
459 sources under acidified conditions, but evidently such an increase in the quality of

460 food could still be insufficient for compensating against calcification declines.

461

462 Feeding is fundamental for marine bivalves to acquire energy, and its plasticity is
463 therefore a prerequisite for acclimation in a rapidly acidifying ocean. As reviewed by
464 Clements and Darrow (2018), many bivalve species experienced depressed feeding
465 rates and thus reduced energy acquisition when exposed to elevated pCO_2. Yet, little
466 information is available about the role played by the food availability, mainly because
467 most laboratory-based experiments are carried out under the same feeding regimes.
468 In the field, previous studies within upwelling systems have demonstrated that food
469 availability could be sufficient for mussels to maintain shell growth and tissue energy
470 reserves, while still fulfilling increased energy demands under acidified conditions
471 (e.g., Parker et al., 2015; Zhao et al., 2018b, 2019a; Ramajo et al., 2020). At CO_2 seeps
472 off Shikine Island, while ocean acidification resulted in marked shifts in ecosystems
473 dominated by turf algae (Harvey et al., 2021a), due to the CO_2 fertilization, turf algae
474 can be more likely to rapidly proliferate than macroalgae outside seeps (Harvey et al.,
475 2021b). The availability of food stemming from predominant turf algal detritus for
476 mussels living around CO_2 seeps might be particularly abundant. The role played by
477 turf algae in the quality and availability of food for mussel consumption deserves
478 further investigation.

479

480 Taken together, considering significant decreases in condition index and shell
481 growth, it is reasonable to assume that evident shifts in dietary regimes which may

482 be beneficial for energy acquisition are not sufficient to fully compensate for the
483 impact of OA on mussel shell formation. As demonstrated below, it is likely that a re-
484 partitioning of energy amongst different shell calcification processes may occur.
485

486 **4.2. Mechanisms of mussel calcification at CO_2 seeps are less energetically efficient**

487 Understanding the sensitivity of calcification to OA requires an appreciation of the
488 regulation of calcifying fluid carbonate chemistry. Identification of sources and
489 pathways of dissolved inorganic carbon (DIC) at the calcifying front has greatly
490 improved our knowledge in this regard. Up to 100% of shell carbonate was
491 composed of seawater DIC suggesting that mussels almost exclusively extract
492 external seawater DIC rather than internal metabolic CO_2 to calcify. While this finding
493 agrees well with the theoretical calculation of the respiratory gas exchange model,
494 whereby seawater DIC contributes more than 90% of the calcifying fluid DIC pool
495 (McConnaughey et al., 1997), evidence is accumulating that marine bivalves,
496 especially under OA stress, can preferentially transport metabolic CO_2 as a more
497 efficient and less costly compensatory mechanism to regulate the carbonate
498 chemistry of their calcifying fluid (e.g., Gillikin et al., 2007; Zhao et al., 2018a; Lu et
499 al., 2019; Lee et al., 2021). Up to 61% of metabolic carbon, for example, was
500 observed in shells of Manila clams (*Ruditapes philippinarum*) which exhibited rapid
501 acclimation to high pCO_2 following transgenerational exposure (Zhao et al., 2018a).
502 Considering that cellular membranes are highly CO_2 permeable (Gutknecht et al.,
503 1977), metabolic CO_2 can passively diffuse into the calcifying fluid, where it is quickly

504 transformed to HCO_3^- through the hydration of carbonic anhydrase (Zhao et al.,
505 2020b). In comparison to the passive diffusion of metabolic CO_2, the transport of
506 seawater DIC for calcification is thought to be energetically expensive, since the
507 active transport of HCO_3^- (the most likely calcification-relevant DIC species in
508 seawater) from the ambient seawater to the calcifying front requires many ion
509 channels, exchangers, and transporters (as reviewed in Zhao et al., 2020a). The
510 reason that mussels inhabiting the elevated pCO_2 conditions have mainly employed
511 mechanisms for active transport of seawater DIC rather than less costly preferential
512 uptake of metabolic CO_2 as calcifying substrates remains unknown, but it is intriguing
513 that the latter usually is seen in bivalves inhabiting intertidal zones where they
514 habitually experience aerial exposure during the low tide and therefore are used to
515 counter respiratory acidosis caused by the retention of metabolic CO_2 (Booth et al.,
516 1984; Burnett, 1988). Since the mussels used here were located in the very low
517 intertidal, it is possible that metabolic CO_2 production during the relatively short
518 aerial exposure is insufficient to maintain calcification rates, necessitating the use of
519 the more energetically-costly seawater-derived HCO_3.
520
521 Active removal of protons generated during the $CaCO_3$ precipitation at the site
522 of calcification is a fundamental requirement for stress tolerance and acclimation to
523 OA. With increasing pCO_2 concentrations, the amounts of pH-sensitive elements such
524 as B and U incorporated into mussel shells decreased significantly, demonstrating
525 declines of pH at the site of calcification. Similar results have been documented in a

526 variety of coastal bivalves acutely exposed to OA scenarios projected by the end of
527 this century (e.g., Heinemann et al., 2012; Frieder et al., 2014; Liu et al., 2015; Zhao
528 et al., 2018b). Perhaps most notably, virtually unaffected Na/Ca_{shell} and K/Ca_{shell} ratios
529 demonstrate that mussels may be unable to complement a suite of less costly and
530 more efficient ion-regulatory machineries equipped in the mantle tissue, especially
531 Na^+/H^+ exchanger (Zhao et al., 2017a; Ramesh et al., 2018), for the removal of
532 excessive protons in the calcifying fluid. If this is the case, then one would expect
533 that energy-requiring H^+-ATPase may play a major role in actively pumping protons
534 out of the site of calcification. Taken together, it is reasonable to assume that mussels
535 collected within the elevated pCO_2 areas do not possess compensatory mechanisms
536 that are energetically efficient in the maintenance of calcifying fluid acid-base
537 homeostasis under OA stress.
538
539 Considering the corrosive nature of acidified waters within the elevated pCO_2
540 areas, it is also imperative to account for the degree to which shell calcification could
541 be counteracted by dissolution and erosion. It has been documented that gastropods,
542 *Charonia lampas*, collected at our study sites exhibited serious shell dissolution and
543 visible deterioration (Harvey et al., 2018), due to loss of periostracum – an external
544 organic cover protecting shells from corrosive seawater (Saleuddin and Petit, 1983).
545 When maintained under elevated pCO_2 conditions for two months, mussels did not
546 lose the thickness of periostracum in the newly formed shell portion and undergo
547 progressive shell dissolution and erosion, indicating that their shell properties may

548 not be as susceptible to seawater acidification as *C. lampas*. Hence, the resilience of
549 marine bivalves to calcify in an acidifying ocean also depends on their ability to
550 counter periostracum loss and shell dissolution. The $\delta^{13}C$ analysis indicates that the
551 formation of mussel periostracum is mediated by organic matrix synthesized and
552 secreted from the outer mantle epithelium (Zhao et al., 2019b), the latter known to
553 be extremely energetically expensive and equivalent to 60% of the energy demands
554 of somatic growth or 150% of the energetic demands of gamete development
555 (Palmer, 1992). The maintenance of periostracum formation thus indicate that under
556 acidified conditions mussels give priority to the shell defence rather than calcification,
557 especially considering that accumulating evidence suggests that the total amount of
558 energy allocated for shell formation declines considerably under acidified conditions,
559 (Waldbusser et al., 2013; Li et al., 2016; Spalding et al., 2017; Leung et al., 2020b).
560 Compensatory mechanisms such as the production of alternative calcium carbonate
561 polymorphs (e.g. Leung et al. 2017) or the production of thicker shells (e.g. Cross et
562 al. 2019) may additionally help to counteract the negative effects of ocean
563 acidification on the shell morphology. By combining findings obtained from reciprocal
564 transplantation (i.e., the limited energy budget, the more energetically costly
565 calcification processes, and the importance of the periostracum in impeding shell
566 dissolution), it is, therefore, reasonable to assume that mussels may be forced to
567 employ functional trade-offs in their energy expenditure in order to survive under
568 elevated pCO_2 conditions.
569

570 **4.3. Mussels shrink to survive under elevated *p*CO_2 conditions**

571 While most calcifiers (oysters, decapods, gastropods, barnacles, etc.) had significant
572 decreases in abundance around the volcanic CO_2 seeps off Shikine Island (Agostini et
573 al., 2018), patchily distributed dense clusters of mussels were seen along the
574 gradients of CO_2, sparking interest in understanding why mussels can survive OA.
575 Limited energy budget, less energy-efficient calcification, and sustained periostracum
576 integrity are traits being exhibited by the mussels following their exposure to
577 elevated *p*CO_2 conditions (Thomsen et al., 2017; Zhao et al., 2017a), which however
578 cannot satisfactorily explain why mussels can survive at CO_2 seeps. High-resolution
579 analysis of shell geochemistry also indicates that mussel calcification is adversely
580 affected by high *p*CO_2. Evidence in support of this assumption comes from the
581 consistently higher values of $\delta^{13}C_{shell}$ profiles than those observed in control mussels,
582 indicating that mussels living near CO_2 seeps incorporate higher amount of seawater
583 inorganic carbon (which had higher $\delta^{13}C$ values than that of metabolic carbon) to the
584 site of calcification than those grown outside seeps. Hence, mussels collected from
585 the elevated *p*CO_2 areas adopted energetically costly strategies (e.g., active transport
586 of seawater DIC rather than the passive diffusion of metabolic carbon) to calcify. The
587 integrity of periostracum also suggests that energy is being allocated for its
588 maintenance, as demonstrated above. In line with findings following reciprocal
589 transplantation, therefore, it is reasonable to assume that mussels suffer a reduced
590 energy budget in acidified conditions.

591

592 Surprisingly, our chronological findings indicate that, despite their small size
593 (shell length 1.86 to 2.83 cm), mussels randomly chosen for reciprocal
594 transplantation were up to 7-years-old. Mussels collected near the CO_2 seeps were
595 not only older, but also grew slower than those living outside the CO_2 seeps, leading
596 to the shell length of mussels being smaller by as much as 20%. Presumably, slow
597 shell building is a strategy used by mussels to survive elevated pCO_2 conditions. A
598 similar observation has been made for two gastropod species at natural CO_2 seeps
599 off Vulcano Island, Italy, whereby the ability to adapt through dwarfing conferred a
600 physiological advantage for the smaller individuals to survive under increased CO_2
601 levels (Garilli et al. 2015).
602
603 Slow shell building can substantially lessen the energy burden of stressed
604 mussels. Similar conclusions have been often drawn on the early life stages of
605 brooding marine bivalves (e.g., Noisette et al., 2014; Lucey et al., 2015; Waldbusser
606 et al., 2016). The rates of calcification and energy consumption in the larvae of
607 brooding oysters *Ostrea lurida* for example are nearly 10 and 50 times slower than
608 those of broadcast spawning oysters *Crassostrea gigas* (Waldbusser et al., 2016).
609 Mechanisms underpinning slow shell building as a possible trait for resistance to OA
610 are suggestively associated with the kinetic-energetic constraint on shell calcification
611 (Waldbusser et al., 2013, 2014). Reductions in body length to decrease energy needs
612 when under harsh conditions has been observed in many organisms (Wikelski and
613 Thom, 2000; Sheridan and Bickford, 2011; Garilli et al. 2015). Smaller body size can

be an advantage as pCO_2 levels continue to rise.

The use of CO_2 seeps in this study allowed us to investigate the consequences of future ocean acidification on mussel shell formation. It should be acknowledged, however, that this is in the absence of concurrent ocean warming (Hughes et al. 2017), and changes in temperature will mediate the response of organisms and communities to future ocean acidification. It may be possible in future studies, for example, to carry out studies that manipulate temperature along CO_2 gradients (e.g., Alessi et al., 2019). Regardless, CO_2 seeps and other natural analogues are still invaluable for assessing the future state of organisms, communities, and ecosystems to future ocean acidification (Rastrick et al., 2018).

5. Conclusions

This study is the first to provide a comprehensive understanding of how mussels calcify and grow at CO_2 seeps off Shikine Island. We observed that mussels inhabiting elevated pCO_2 conditions exhibited marked shifts in their food sources, and displayed significant decreases in their condition index and hence tissue energy reserves. While the mussels were able to survive, their shell formation was negatively impacted by ocean acidification, leading to reduced growth and size. They survived through slow shell building, demonstrated by high-resolution analysis of shell geochemistry over their lifespan. This slow shell growth is a plastic response that allows them to maintain a smaller body size, a physiological advantage to enhance energy efficiency.

These findings reveal future trajectories for marine bivalves in an acidifying ocean and provide insights into their scope for acclimation.

Acknowledgments

We thank the technical staff at Shimoda Marine Research Center, University of Tsukuba for their assistance aboard RV Tsukuba II and at the study site, and the Japan Fisheries agencies of Nijima/Shikine Island (Tokyo prefecture) for their support. This project was supported by the 'International Education and Research Laboratory Program', University of Tsukuba, and contributes towards the International CO_2 Natural Analogues (ICONA) Network. This work was also supported by JSPS KAKENHI Grant Number 17K17622 and 17P17333, and we also acknowledge funding support from the Ministry of Environment, Government of Japan (Suishinhi: 4RF-1701), the National Natural Science Foundation of China (42076121, M-0163, 42211530423), the Guangdong Zhujiang Talents Program (2021QN02H665), the Department of Education of Guangdong Province (2020KTSCX050, 2022ZDZX4012) and the program for Scientific Research Start-up Funds of Guangdong Ocean University.

Data Availability Statement

The data that support the findings of this study are openly available in PANGAEA.

References

Agostini, S., Harvey, B.P., Wada, S., Kon, K., Milazzo, M., Inaba, K., Hall-Spencer, J.M.,

2018. Ocean acidification drives community shifts towards simplified non-calcified habitats in a subtropical-temperate transition zone. Sci. Rep. 8, 111354.

Agostini, S., Houlbrèque, F., Biscéré, T., Harvey, B. P., Heitzman, J. M., Takimoto, R., Yamazaki, W., Milazzo, M., Rodolfo-Metalpa, R., 2021. Greater mitochondrial energy production provides resistance to ocean acidification in "winning" hermatypic corals. Front. Mar. Sci. *7*, 1235.

Agostini, S., Wada, S., Kon, K., Omori, A., Kohtsuka, H., Fujimura, H., Tsuchiya, Y., Sato, T., Shinagawa, H., Yamada, Y., Inaba, K., 2015. Geochemistry of two shallow CO_2 seeps in Shikine Island (Japan) and their potential for ocean acidification research. Reg. Stud. Mar. Sci. 2, 45-53.

Aiuppa, A., Hall-Spencer, J. M., Milazzo, M., Turco, G., Caliro, S., Di Napoli, R., 2021. Volcanic CO_2 seep geochemistry and use in understanding ocean acidification. Biogeochemistry 152, 93-115

Alessi, C., Giomi, F., Furnari, F., Sarà, G., Chemello, R., Milazzo, M., 2019. Ocean acidification and elevated temperature negatively affect recruitment, oxygen consumption and calcification of the reef-building *Dendropoma cristatum* early life stages: Evidence from a manipulative field study. Science of The Total Environment, 693, 133476.

Blunden, J., Derek, S.A., Hartfield, G., 2018. State of the climate in 2017. Bull. Am. Meteorol. Soc. 99.

Booth, C.E., McDonald, D.G., Walsh, P.J., 1984. Acid-base balance in the sea mussel, *Mytilus edulis*. II: effects of hypoxia and air-exposure on hemolymph acid-base

status. Mar. Biol. Lett. 5, 359-369.

Burnett, L.E., 1988. Physiological responses to air exposure: acid-base balance and the role of branchial water stores. Am. Zool. 28, 125-135.

Byrne, M., Foo, S.A., Ross, P.M., Putnam, H.M., 2020. Limitations of cross- and multigenerational plasticity for marine invertebrates faced with global climate change. Global Change Biol. 26, 80-102.

Caldeira, K., Wickett, M.E., 2003. Oceanography: anthropogenic carbon and ocean pH. Nature 425, 365.

Clements, J.C., Darrow, E.S., 2018. Eating in an acidifying ocean: a quantitative review of elevated CO_2 effects on the feeding rates of calcifying marine invertebrates. Hydrobiologia 820, 1-21.

Cross, E.L., Harper, E.M., Peck, L.S., 2019. Thicker shells compensate extensive dissolution in brachiopods under future ocean acidification. Environmental Science & Technology, 53(9), 5016–5026.

Dudgeon D., Morton B., 1982. Coral associated Mollusca of Tolo Harbour, Hong Kong. Morton B., Tseng C.K. (Eds.), Proceedings of the First International Marine Biological Workshop: The Marine Flora and Fauna of Hong Kong and southern China, Hong Kong, Hong Kong University Press, Hong Kong, pp. 627-650.

Ekstrom, J.A., Suatoni, L., Cooley, S.R., Pendleton, L.H., Waldbusser, G.G., Cinner, J.E., Ritter, J., Langdon, C., Hooidonk, R.V., Gledhill, D., Wellman, K., Beck, M.W., Brander, L.M., Rittschof, D., Doherty, C., Edwards, P., Portela, R., 2015. Vulnerability and adaptation of US shellfisheries to ocean acidification. Nat. Clim.

Change 3, 207-214.

Feely, R.A., Sabine, C.L., Hernandez-Ayon, J.M., Ianson, D., Hales, B., 2008. Evidence for up-welling of corrosive “acidified” water onto the continental shelf. Science 320, 1490-1492.

Fitzer, S.C., Caldwell, G.S., Phoenix, V.R., Kamenos, N.A., 2014. Ocean acidification reduces the crystallographic control in juvenile mussel shells. J. Struct. Biol. 188, 39-45.

Frieder, C.A., Gonzalez, J.P., Levin, L.A., 2014. Uranium in larval shells as a barometer of molluscan ocean acidification exposure. Environ. Sci. Technol. 48, 6401-6408.

Garilli, V., Rodolfo-Metalpa, R., Scuderi, D., Brusca, L., Parrinello, D., Rastrick, S.P.S., Foggo, A., Twitchett, R.J., Hall-Spencer, J.M., Milazzo, M., 2015. Physiological advantages of dwarfing in surviving extinctions in high-CO_2 oceans. Nature Climate Change, 5(7), 678–682.

Gillikin, D.P., Lorrain, A., Meng, L., Dehairs, F., 2007. A large metabolic carbon contribution to the $\delta^{13}C$ record in marine aragonitic bivalve shells. Geochim. Cosmochim. Acta 71, 2936-2946.

Gutknecht, J., Bisson, M.J., Tosteson, F.C., 1977. Diffusion of carbon dioxide through lipid bilayer membranes: effects of carbonic anhydrase, bicarbonate, and unstirred layers. J. Gen. Physiol. 55, 1-17.

Hahn, S., Rodolfo-Metalpa, R., Griesshaber, E., Schmahl, W.W., Buhl, D., Hall-Spencer, J.M., Baggini, C., Fehr, K.T., Immenhauser, A., 2012. Marine bivalve shell geochemistry and ultrastructure from modern low pH environments:

Environmental effect versus experimental bias. Biogeosciences, 9(5), 1897–1914.

Hall-Spencer, J.M., Rodolfo-Metalpa, R., Martin, S., Ransome, E., Fine, M., Turner, S.M., Rowley, S.J., Tedesco, D., Buia, M.C., 2008. Volcanic carbon dioxide vents show ecosystem effects of ocean acidification. Nature 454, 96-99.

Hall-Spencer, J.M., Belfiore, G., Tomatsuri, M., Porzio, L., Harvey, B.P., Agostini, S., Kon, K., 2022. Decreased diversity and abundance of marine invertebrates at CO_2 seeps in warm-temperate Japan. Zoological Science 39, 41-51.

Harvey, B.P., Agostini, S., Wada, S., Inaba, K., Hall-Spencer, J.M., 2018. Dissolution: the Achilles's hell of the triton shell in an acidifying ocean. Front. Mar. Sci. 5, 371.

Harvey, B.P., Allen, R., Agostini, S., Hoffmann, L.J., Kon, K., Summerfield, T.C., Wada, S., Hall-Spencer, J.M., 2021a. Feedback mechanisms stabilise degraded turf algal systems at a CO_2 seep site. Communications Biol. 4, 219.

Harvey, B.P., Kerfahi, D., Jung, Y., Shin, J.-H., Adams, J.M., Hall-Spencer, J.M., 2020. Ocean acidification alters bacterial communities on marine plastic debris. Mar. Pollut. Bull. 161, 111749.

Harvey, B.P., Kon, K., Agostini, S., Wada, S., Hall-Spencer, J.M., 2021b. Ocean acidification locks algal communities in a species-poor early successional stage. Global Change Biol. 27, 2174-2187.

Harvey, B.P., McKeown, N.J., Rastrick, S.P.S., Bertolini, C., Foggo, A., Graham, H., Hall-Spencer, J.M., Milazzo, M., Shaw, P.W., Small, D.P., Moore, P.J., 2016. Individual and population-level responses to ocean acidification. Scientific Reports, 6(1), 20194.

He, G., Xiong, X., Peng, Y., Yang, C., Xu, X., Liu, X., Liang, J., Masanja, F., Yang, K., Xu, X., Zheng, Z., Deng, Y., Leung, J.Y.S., Zhao, L., 2023. Transcriptomic responses reveal impaired physiological performance of the pearl oyster following repeated exposure to marine heatwaves. Sci. Total Environ. 854, 158726.

Heinemann, A., Fietzke, J., Melzner, F., Bohm, F., Thomsen, J., Garbe-Schonberg, D., Eisenhauer, A., 2012. Conditions of *Mytilus edulis* extracellular body fluids and shell composition in a pH-treatment experiment: acid-base status, trace elements and δ^{11}B. G-cubed 13.

Higo, S., Callomon, P. and Goto, Y., 1999. Catalogue and Bibliography of the Marine Shell-Bearing Mollusca of Japan. Gastropoda. Bivalvia. Polyplacophora. Scaphopoda, Elle Sci. Publ.

Hughes, T.P., Barnes, M.L., Bellwood, D.R., Cinner, J.E., Cumming, G.S., Jackson, J.B.C., Kleypas, J., van de Leemput, I.A., Lough, J.M., Morrison, T.H., Palumbi, S.R., van Nes, E.H., Scheffer, M., 2017. Coral reefs in the Anthropocene. Nature 546, 82–90.

Hüning, A.K., Melzner, F., Thomsen, J., Gutowska, M.A., Krämer, L., Frickenhaus, S., Rosenstiel, P., Pörtner, H.O., Philipp, E.E.R., Lucassen, M., 2013. Impacts of seawater acidification on mantle gene expression patterns of the Baltic Sea blue mussel: implications for shell formation and energy metabolism. Mar. Biol. 160, 1845-1861.

Inoue, S., Kayanne, H., Yamamoto, S., Kurihara, H., 2013. Spatial community shift from hard to soft corals in acidified water. Nat. Clim. Chang. 3, 683-687.

IPCC, 2013. Summary for policymakers. In: Stocker, T.F., Qin, D., Plattner, G.-K., Tignor, M., Allen, S.K., Boschung, J., Nauels, A., Xia, Y., Bex, V., Midgley, P.M. (Eds.), Climate Change 2013: the Physical Science Basis. Contribution of Working Group I to the Fifth Assessment Report of the Intergovernmental Panel on Climate Change. Cambridge University Press, Cambridge, United Kingdom and New York, NY, USA, pp. 1-30.

Kerfahi, D., Harvey, B.P., Agostini, S., Kon, K., Huang, R., Adams, J.M., Hall-Spencer, J.M., 2020. Responses of intertidal bacterial biofilm communities to increasing pCO_2. Mar. Biotechnol. 22, 727-738.

Lee, T.H., McGill, R.A.R., Fitzer, S., 2021. Effects of extra feeding combined with ocean acidification and increased temperature on the carbon isotope values ($\delta^{13}C$) in the mussel shell. J. Exp. Mar. Biol. Ecol. 541, 151562.

Leung, J.Y.S., Chen, Y., Nagelkerken, I., Zhang, S., Xie, Z., Connell, S.D., 2020a. Calcifiers can adjust shell building at the nanoscale to resist ocean acidification. Small 16, 2003186.

Leung, J.Y.S., Doubleday, Z.A., Nagelkerken, I., Chen, Y., Xie, Z., Connell, S.D., 2019. How calorie-rich food could help marine calcifiers in a CO_2-rich future. Proc. R. Soc. B 286, 20190757.

Leung, J.Y.S., Nagelkerken, I., Russell, B.D., Ferreira, C.M., Connell, S. D., 2018. Boosted nutritional quality of food by CO_2 enrichment fails to offset energy demand of herbivores under ocean warming, causing energy depletion and mortality. Science of the Total Environment, 639, 360–366.

Leung, J.Y.S., Russell, B.D., Connell, S.D., 2017. Mineralogical plasticity acts as a compensatory mechanism to the impacts of ocean acidification. Environmental Science & Technology, 51(5), 2652–2659.

Leung, J.Y.S., Russell, B.D., Connell, S.D., 2020. Linking energy budget to physiological adaptation: how a calcifying gastropod adjusts or succumbs to ocean acidification and warming. Sci. Total Environ. 715, 136939.

Leung, J.Y.S., Zhang, S., Connell, S.D., 2022. Is ocean acidification really a threat to marine calcifiers? A systematic review and meta-analysis of 980+ studies spanning two decades. Small 18, 2107407.

Levin, L.A., Hönisch, B., Frieder, C.A., 2015. Geochemical proxies for estimating faunal exposure to ocean acidification. Geochemistry 28, 62-73.

Li, S., Liu, C., Huang, J., Liu, Y., Zhang, S., Zheng, G., Xie, L., Zhang, R., 2016. Transcriptome and biomineralization responses of the pearl oyster *Pinctada fucata* to elevated pCO_2 and temperature. Sci. Rep. 6, 18493.

Liu, Y.W., Aciego, S.M., Wanamaker, A.D., 2015. Environmental controls on the boron and strontium isotopic composition of aragonite shell material of cultured *Arctica islandica.* Biogeosciences 12, 3351-3368.

Liu, Y., Sutton, J.N., Ries, J.B., Eagle, R.A., 2020. Regulation of calcification site pH is a polyphyletic but not always governing response to ocean acidification. Sci. Adv. 6, eaax1314.

Lu, Y., Wang, L., Wang, L., Cong, Y., Yang, G., Zhao, L., 2018. Deciphering carbon sources of mussel shell carbonate under experimental ocean acidification and

warming. Mar. Environ. Res. 142, 141-146.

Lucas, A., Beninger, P.G., 1985. The use of physiological condition indices in marine bivalve aquaculture. Aquaculture 44, 187-200.

Lucey, N.M., Lombardi, C., DeMarchi, L., Schulze, A., Gambi, M.C., Calosi, P., 2015. To brood or not brood: are marine invertebrates that protect their offspring more resilient to ocean acidification? Sci. Rep. 5, 12009.

Marin, F., Le Roy, N., Marie, B., 2012. The formation and mineralization of mollusk shell. Front. Biosci. S4, 1099-1125.

Martins, M., Carreiro-Silva, M., Martins, G.M., e Ramos, J.B., Viveiros, F., Couto, R.P., Parra, H., Monteiro, J., Gallo, F., Silva, C., Teodosio, A., Guilini, K., Hall-Spencer, J.M., Leitao, F., Chicharo, L., Range, P., 2021. *Ervilia castanea* (Mollusca, Bivalvia) populations adversely affected at CO_2 seeps in the North Atlantic. Sci. Total Environ. 754, 142044.

McConnaughey, T.A., Burdett, J., Whelan, J.F., Paull, C.K., 1997. Carbon isotopes in biological carbonates: respiration and photosynthesis. Geochem. Cosmochim. Acta 61, 611-622.

Melzner, F., Mark, F.C., Seibel, B.A., Tomanek, L., 2020. Ocean acidification and coastal marine invertebrates: tracking CO_2 effects from seawater to the cell. Annual Rev. Marine Sci. 12, 499-523.

Morton, B., 2019. The biology and functional morphology of *Septifer bilocularis* and *Mytilisepta virgata* (Bivalvia: Mytiloidea) from corals and the exposed rocky shores, respectively, of Hong Kong. Regional Studies in Marine Science 25,

100454.

Morton, B., Leung, P.T.Y., Wei, J., Lee, G.Y., 2020. A morphological and genetic comparison of *Septifer bilocularis*, *Mytilisepta virgata* and *Brachidontes variabilis* (Bivalvia: Mytiloidea) from Hong Kong and erection of the Mytiliseptiferinae sub-fam. nov. Regional Studies in Marine Science 34, 100981.

Noisette, F., Comtet, T., Legrand, E., Bordeyne, F., Davoult, D., Martin, S., 2014. Does encapsulation protect embryos from the effects of ocean acidification? The example of *Crepidula fornicata*. PLoS One 9, 1-11.

Palmer, A.R., 1992. Calcification in marine molluscs: how costly is it? Proc. Natl. Acad. Sci. U. S. A. 89, 1379-1382.

Parker, L.M., O'Connor, W.A., Raftos, D.A., Pörtner, H.O., Ross, P.M., 2015. Persistence of positive carryover effects in oysters following transgenerational exposure to ocean acidification. PloS One 10, e0132276.

Pierrot, D.E., Lewis, E., Wallace, D.W.R., 2006. MS Excel Program Developed for CO_2 System Calculations, ORNL/CDIAC-105a, Carbon Dioxide Information Analysis Center. Oak Ridge National Laboratory, U.S. Department of Energy, Oak Ridge, Tennessee.

Rajan, K.C., Meng, Y., Yu, Z., Roberts, S.B., Vengatesen, T., 2021. Oyster biomineralization under ocean acidification: from genes to shell. Glob. Chang. Biol. 27, 3779-3797.

Ramajo, L., Pérez-Léon, E., Hendriks, I.E., Marbà, N., Krause-Jensen, D., Sejr, M.K., Blicher, M.E., Lagos, N.A., Olsen, Y.S., Duarte, C.M., 2016. Food supply confers

calcifiers resistance to ocean acidification. Sci. Rep. 6, 19374.

Ramesh, K., Yarra, T., Clark, M.S., John, U., Melzner, F., 2019. Expression of calcification- related ion transporters during blue mussel larval development. Ecol. Evol. 9, 7157-7172.

Rastrick, S.S.P., Graham, H., Azetsu-Scott, K., Calosi, P., Chierici, M., Fransson, A., et al., 2018. Using natural analogues to investigate the effects of climate change and ocean acidification on northern ecosystems. ICES J. Mar. Sci. 75, 2299-2311.

Récluz C.A., 1848. Description d'un nouveau genre de coquille bivalve nommé Septifère (Septifer). Rev. Zool. Soc. Cuv. 11, 275-279

Reusch, T.B.H., 2014. Climate change in the oceans: evolutionary versus phenotypically plastic responses of marine animals and plants. Evol. Appl. 7, 104-122.

Ricevuto, E., Vizzini, S., Gambi, M.C., 2015. Ocean acidification effects on stable isotope signatures and trophic interactions of polychaete consumers and organic matter sources at a CO_2 shallow vent system. Journal of Experimental Marine Biology and Ecology 468, 105-117.

Ross, P.M., Parker, L., Byrne, M., 2016. Transgenerational responses of molluscs and echinoderms to changing ocean conditions. ICES J. Mar. Sci. 73, 537-549.

Saleuddin, A.S.M., Petit H.P., 1983. The mode of formation and the structure of the periostracum. In Physiology, Part 1 The Mollusca, vol. 4 (eds. Saleuddin, A.S.M., Wilbur, K.M.). Academic Press, New York, pp. 199-234.

Sheridan, J.A., Bickford, D., 2011. Shrinking body size as an ecological response to

climate change. Nat. Clim. Change 1, 401-406.

Sillanpää, J.K., Sundh, H., Sundell, K.S., 2018. Calcium transfer across the outer mantle epithelium in the Pacific oyster, Crassostrea gigas. Proc. R. Soc. B 285, 20181676.

Spalding, C., Finnegan, S., Fischer, W.W., 2017. Energetic costs of calcification under ocean acidification. Global Biogeochem. Cycles 31, 866-877.

Thomsen, J., Stapp, L.S., Haynert, K., Schade, H., Danelli, M., Lannig, G., Wegner, K.M., Melzner, F., 2017. Naturally acidified habitat selects for ocean acidification-tolerant mussels. Sci. Adv. 3, e1602411.

Waldbusser, G.G., Brunner, E.L., Haley, B.A., Hales, B., Langdon, C.J., Prahl, F.G., 2013. A developmental and energetic basis linking larval oyster shell formation to acidification sensitivity. Geophys. Res. Lett. 40, 2171-2176.

Waldbusser, G.G., Hales, B., Langdon, C.J., Haley, B.A., Schrader, P., Brunner, E.L., Gray, M.W., Miller, C.A., Gimenez, I., 2014. Saturation-state sensitivity of marine bivalve larvae to ocean acidification. Nat. Clim. Change 5, 273-280.

Waldbusser, G.G., Gray, M.W., Hales, B., Langdon, C.J., Haley, B.A., Gimenez, I., Smith, S.R., Brunner, E.L., Hutchinson, G., 2016. Slow shell building, a possible trait for resistance to the effects of acute ocean acidification. Limnol. Oceanogr. 61, 1969-1983.

Witkowski, C. R., Agostini, S., Harvey, B. P., van der Meer, M. T. J., Sinninghe Damsté, J. S., Schouten, S., 2019. Validation of carbon isotope fractionation in algal lipids as a pCO_2 proxy using a natural CO_2 seep (Shikine Island, Japan). Biogeosciences,

16, 4451–4461.

Wikelski, M., Thom, C., 2000. Marine iguanas shrink to survive El Nino. Nature 403, 37-38.

Zhao, L., Liu, B., An, W., Deng, Y., Lu, Y., Liu, B., Wang, L., Cong, Y., Sun, X., 2019a. Assessing the impact of elevated pCO_2 within and across generations in a highly invasive fouling mussel (*Musculista senhousia*). Sci. Total Environ. 689, 322-333.

Zhao, L., Lu, Y., Yang, F., Liang, J., Deng, Y., 2020b. Transgenerational biochemical effects of seawater acidification on the Manila clam (*Ruditapes philippinarum*). Sci. Total Environ. 710, 136420.

Zhao, L., Milano, S., Walliser, E.O., Schöne, B.R., 2018b. Bivalve shell formation in a naturally CO_2-enriched habitat: unraveling the resilience mechanisms from elemental signatures. Chemosphere 203, 132-138.

Zhao, L., Schöne, B.R., Mertz-Kraus, R., Yang, F., 2017a. Insights from sodium into the impacts of elevated pCO_2 and temperature on bivalve shell formation. J. Exp. Mar. Biol. Ecol. 486, 148-154.

Zhao, L., Schöne, B.R., Mertz-Kraus, R., Yang, F., 2017b. Sodium provides unique insights into transgenerational effects of ocean acidification on bivalve shell formation. Sci. Total Environ. 577, 360-366.

Zhao, L., Shirai, K., Tanaka, K., Milano, S., Higuchi, T., Murakami-Sugihara, N., Walliser, E.O., Yang, F., Deng, Y., Schöne, B.R., 2020a. A review of transgenerational effects of ocean acidification on marine bivalves and their implications for sclerochronology. Estuar. Coast. Shelf S., 235, 106620.

Zhao, L., Shirai, K., Murakami-Sugihara, N., Higuchi, T., Tanaka, K., 2019b. Mussel periostracum as a high-resolution archive of soft tissue δ13C records in coastal ecosystems. Geochem. Cosmochim. Acta 260, 232-243.

Zhao, L., Yang, F., Milano, S., Han, T., Walliser, E.O., Schöne, B.R., 2018a. Transgenerational acclimation to seawater acidification in the Manila clam *Ruditapes philippinarum*: preferential uptake of metabolic carbon. Sci. Total Environ. 627, 95-103.

Zhao, L., Yang, F., Yan, X., 2013. Stable isotopes and fatty acids as dietary tracers of intertidal bivalves. Fisheries Sci. 79, 749-756.

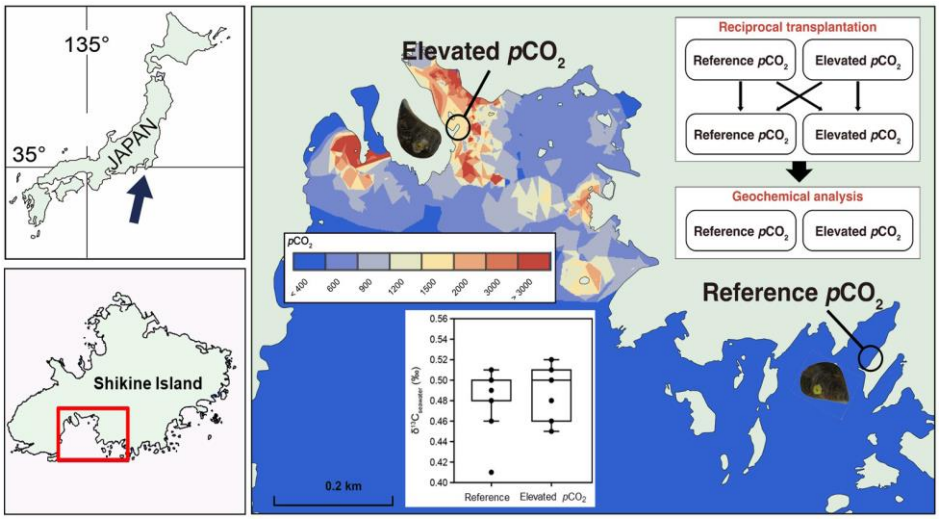

Figure 1 Volcanic CO_2 seeps off Shikine Island (Japan) showing the spatial variability in seawater pCO_2 (based on data by Agostini et al. 2018 using ArcGIS 10.2 software) and the average $\delta^{13}C$ ratio of seawater DIC near and outside the CO_2 seeps (based on data collected during the survey in October 2019). Experimental design showing reciprocal transplantation and high-resolution analysis of shell geochemistry of mussels (*Septifer bilocularis*) collected from the reference and elevated pCO_2 sites. Mussels were labelled with a reference number using queen bee marking tags for identification.

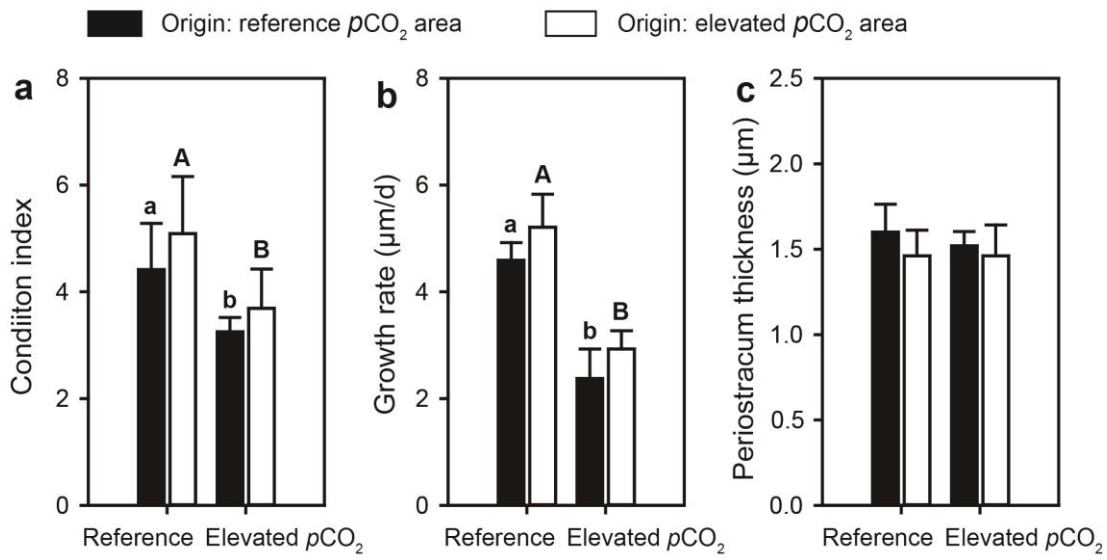

Figure 2 Growth performance of mussels collected from the reference pCO_2 and elevated pCO_2 areas following reciprocal transplantation. (a) condition index; (b) growth rate; (c) the thickness of periostracum. Solid black fill indicates that individuals originated from reference pCO_2 area, and solid white fill indicates that individuals originated from elevated pCO_2 area. Small letters indicate a significant difference in mussels originating from the reference pCO_2 area under reference and elevated pCO_2 conditions, and capital letters indicates significant differences in those mussels originally collected from the elevated pCO_2 area.

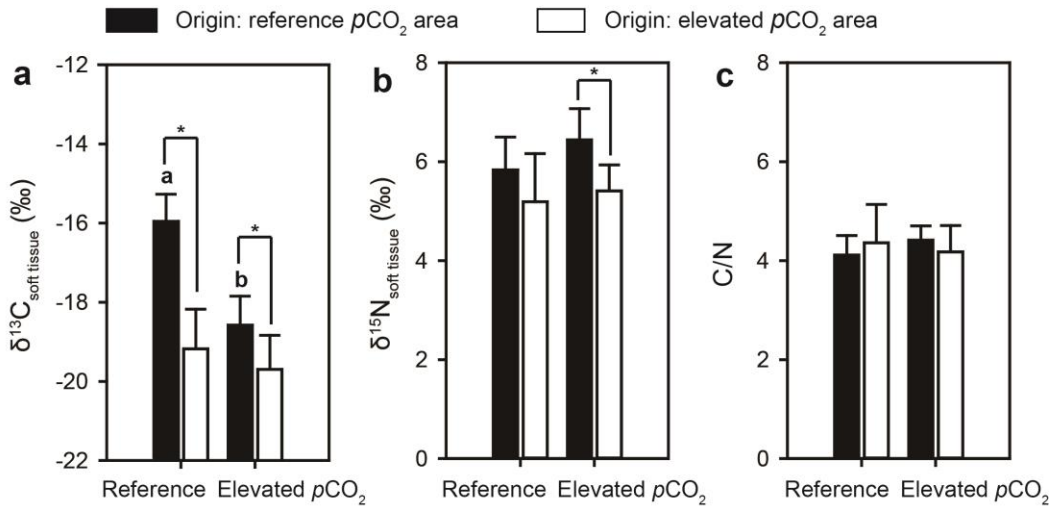

Figure 3 Somatic stable isotopic signatures of mussels from the reference pCO_2 and elevated pCO_2 areas following reciprocal transplantation. (a) stable carbon isotope ($\delta^{13}C$); (b) stable nitrogen isotope ($\delta^{15}N$); (c) C/N. Small letters indicate a significant difference in mussels collected from the reference pCO_2 area under low and high pCO_2 conditions, and an asterisk indicates a significant difference between reciprocally transplanted mussels subjected to the same pCO_2 scenario.

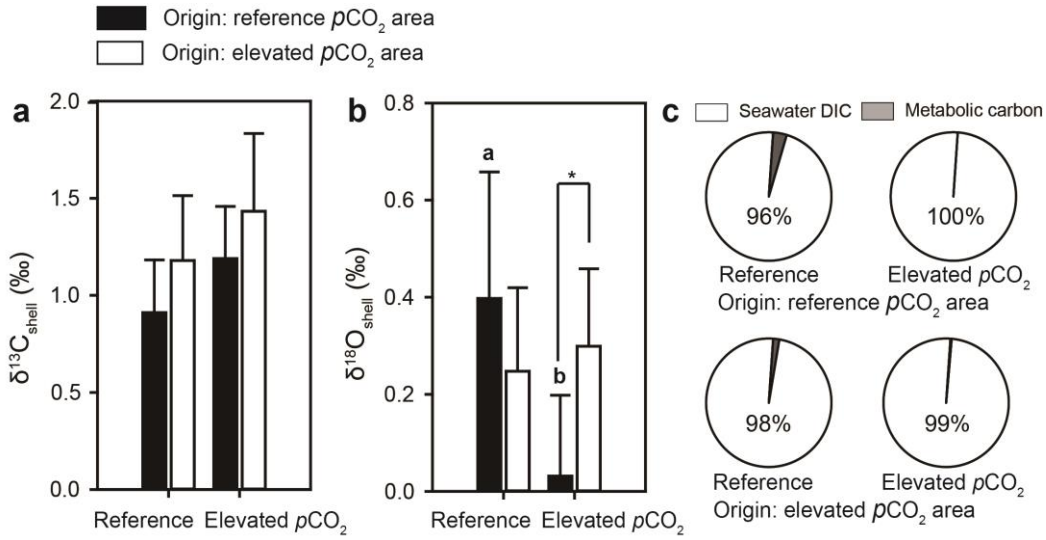

Figure 4 Shell geochemical properties of mussels from the reference pCO_2 and elevated pCO_2 areas following reciprocal transplantation. (a) stable carbon isotope ($\delta^{13}C$); (b) stable oxygen isotope ($\delta^{18}O$); (c) relative contribution of seawater DIC and metabolic carbon to shell carbonate. Small letters indicate a significant difference in mussels collected from the reference pCO_2 area under low and high pCO_2 conditions, and an asterisk indicates a significant difference between reciprocally transplanted mussels subjected to the same pCO_2 scenario.

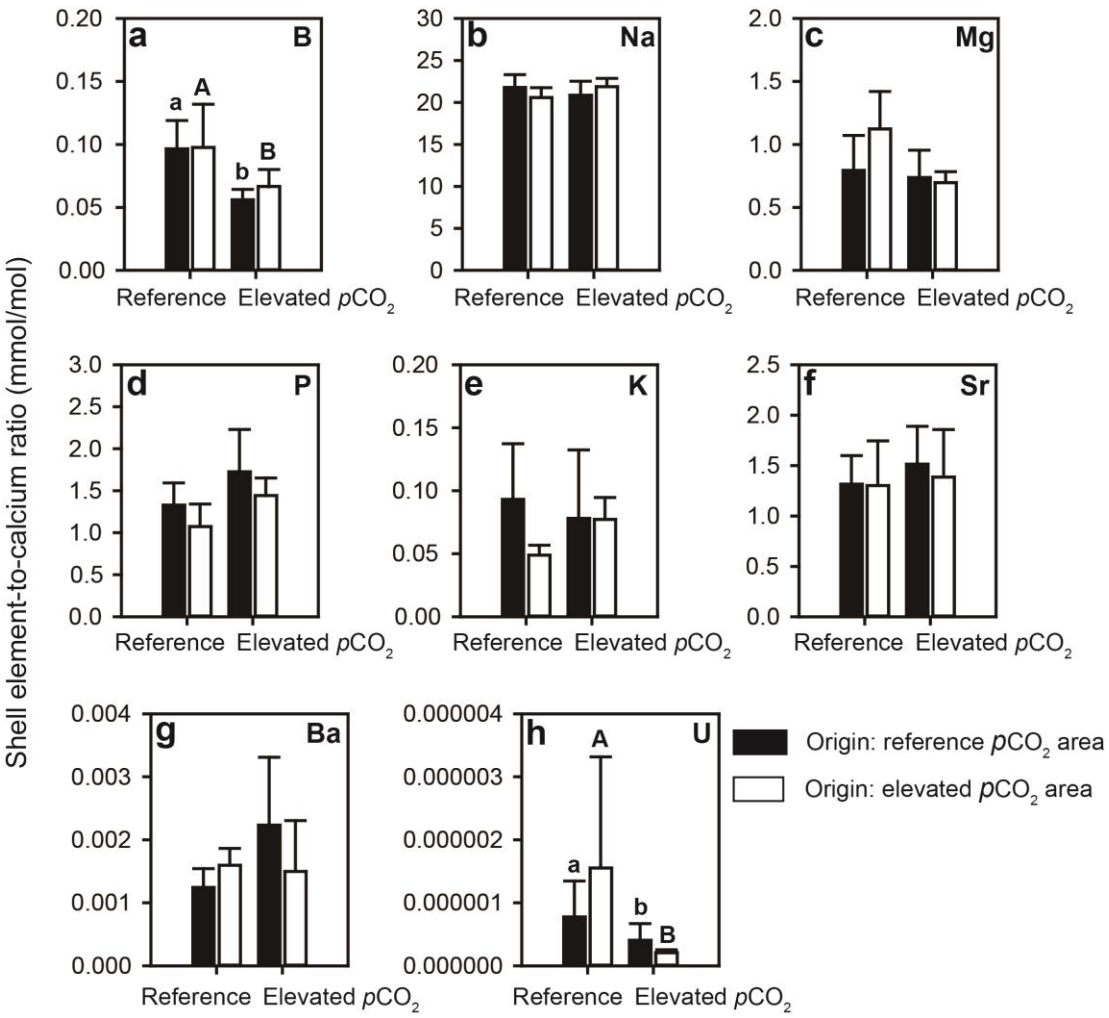

Figure 5 Shell element-to-calcium ratios of mussels collected from the reference pCO_2 and elevated pCO_2 areas following reciprocal transplantation. (a) B/Ca; (b) Na/Ca; (c) Mg/Ca; (d) P/Ca; (e) K/Ca; (f) Sr/Ca; (g) Ba/Ca; (h) U/Ca. Small letters indicate a significant difference in mussels originating from the reference pCO_2 area under reference and elevated pCO_2 conditions, and capital letters indicates significant differences in those mussels originally collected from the elevated pCO_2 area.

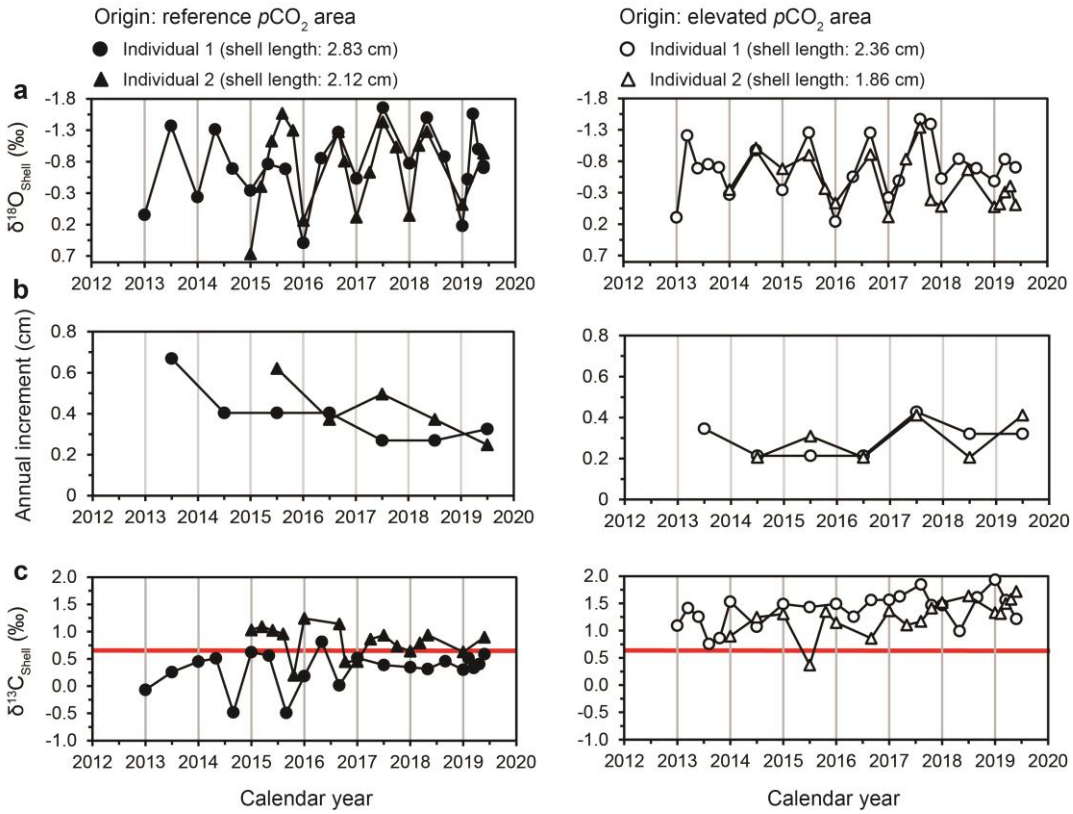

Figure 6 Analysis of shell geochemistry in mussels collected from the reference pCO_2 and elevated pCO_2 areas. Two individuals were selected from the reciprocal transplant experiment for further analysis. This used only those procedural control individuals that had been collected from, and transplanted back into the same site. (a) stable oxygen isotope ($\delta^{18}O$) of mussel shells according to which each shell portion was placed into a temporal context and ontogenetic age of each mussel was then determined; (b) annual increment calculated according to the temporal aligned shell portion; (c) stable carbon isotope ($\delta^{13}C$) of mussel shells. Red lines indicate the mean $\delta^{13}C$ ratio of seawater DIC in the reference pCO_2 and elevated pCO_2 areas.